PAPER 8 (SESSION I)

Fully plastic crack growth under monotonic and repeated bending

HELMUT W. HUFF,* JAMES A. JOYCE,† and FRANK A. McCLINTOCK,†
*Karl Gayer Str. 11, 8 Munchen 50
† Massachusetts Institute of Technology, Cambridge, Mass., U.S.A.

Summary
The stress, strain and displacement fields are given for plane-strain crack growth under an arbitrary deformation history in non-strainhardening, doubly grooved, bending specimens with angles small enough to give slip on only one pair of surfaces.

An 'apparent crack ductility,' observable fracto-graphically, is defined as the ratio of that part of the projected crack area exposed by pure plastic flow to the total projected area, including that exposed by fracture. The apparent crack ductility is related to the crack opening angle and to the crack advance per unit applied deformation. Crack angles, apparent crack ductilities, and low-cycle fatigue striations on aluminum bars and steel bars were consistent with the analysis.

Introduction

While elastic-plastic crack growth seems to be the most urgent problem of fracture, the distributions of stress and strain for fully plastic growth are much more easily found. Such fractures may occur in metal working and in structures loaded nearly to their limit loads. Finally, certain kinds of fully plastic behavior may be representative of the material at the very tip of a crack in an elastic-plastic continuum [1, 4].

We shall study stress and strain at points distant enough from the tip of the crack so that the ordinary theory of homogeneous, isotropic, non-hardening plasticity applies. Very close to the tip, the effects of inhomogeneities, blunting, strain gradients, blunting, the fracture process itself, and perhaps strain-hardening become more important. The results obtained here should provide boundary conditions to such very localized processes. At the same time, the processes at the tip of the crack supply boundary conditions to the remaining material, so we shall need to see how the local behavior affects the macroscopic.

A. P. Green [5] showed that for plane strain specimens in bending, whenever the flank angle is less than 30° for doubly grooved specimens or 3·2° for singly grooved specimens, the slip line field consists of just two arcs that break through to the tip of the groove. It is shown in the appendix that for larger groove angles, containing fans, the displacement fields nearly coincide with those for slip on a single pair of arcs. Since the simpler slip line field can be integrated much more easily under fatigue loading, we shall study that case and consider only the doubly grooved specimens, for

which the simple field occurs or is a good approximation over a much wider range of angles.

Influence of processes at the tip of the groove

The macroscopic flow field is shown in Fig. 1. Near the tip, the curvature of the slip lines may be neglected, so the following discussion applies to unequally grooved or singly grooved tensile specimens in which a single pair of slip planes intersects the tip of the groove. The local processes at the tip affect the macroscopic flow field through the rate at which the active slip surfaces advance into the material and through the symmetry of the flow. For instance, with simultaneous slip on the two surfaces there will be no advance, whereas with pure cleavage on the central plane the advance will be infinitely rapid and there will be no strain. A third extreme form of behavior would be fracture along one of the shear surfaces, corresponding to the shear lip in fracture of thick plates or the cup- and cone fracture in the tensile test.

Simultaneous sliding on the two slip surfaces, which is likely to occur in materials with a dependence of the flow stress on the strain rate leads to a blunted tip and no advance of the slip plane. This will not be considered further because it has not been observed, either here, in the singly grooved tensile fracture [6], or in the similar double cup tensile fracture in very ductile materials [7].

Alternating sliding off, which is likely to occur in strain-hardening materials where sliding off reveals fresh material, does advance the slip surfaces. This process, along with concurrent cleavage, is illustrated in Fig. 2. The crack tip proceeds from O to O′ by cleavage. Sliding up to the right takes the tip to O″. Strain-hardening tends to divert further sliding downward to the right, taking the tip to O‴. The same macroscopic result is obtained for 'shear' fracture along each slip surface in turn, with each step having a projected area on the macroscopic fracture plane that is just half that of the cleavage shown in Fig. 2. No change in direction gives a macroscopic shear fracture (actually combined shear and tension). In the analysis that follows, only the macroscopically normal fracture will be considered.

Macromechanics

(a) *Slip line field*

Consider the specimen as being bent so the left-hand groove is fracturing (f) and the right-hand is closing (c), as shown in Fig. 1. For any flank angle less than $\omega = \pm 30°$, the two circular arcs intersect the groove at an angle of $\lambda = \pm 66{\cdot}8°$ [5]. Their radius R is proportional to the total, or load-carrying part of the ligament, expressed in terms of its half-thickness, L^P.

$$R = (l_f^P + l_c^P)/2 \sin\lambda = L^P/\sin = 1{\cdot}090\, L^P. \qquad (1)$$

(b) *Stress, strain and rotation fields*

The normal stress across the opening and closing slip lines is found by integrating the slip line equations from the center where the normal stress is zero:

$$\sigma/k = \pm\, 2\lambda = \pm\, 2{\cdot}332, \qquad (2)$$

rather low compared with the value $1 + \pi = 4{\cdot}14$ for a zero angle, doubly grooved tensile specimen. (The singly grooved bending specimen does give higher triaxiality, $\sigma/k = 3{\cdot}086$.)

The local strain is found from the displacements across the slip band in one cycle of cleavage and slip, as shown in Fig. 2:

$$\gamma = R\,\dot{\phi}/(\dot{c} + 2R\,\dot{\phi}\cos\lambda)\sin\lambda,$$
$$= 1/(\cot\lambda + \cot\omega_f)\sin^2\lambda = 1{\cdot}18/(0{\cdot}428 + \cot\omega_f). \qquad (3)$$

On the fracturing side, the flank angle is a function of the stress, strain, and rotation (of the stress field relative to a material element), ϕ_σ:

$$\omega_f = \omega_f\,(\sigma/k,\ \gamma,\ \phi_\sigma). \qquad (4)$$

The rotation in the shear band is

$$|\dot{\phi}_\sigma| = |\dot{\gamma}|/2. \qquad (5)$$

The important difference between this rotation rate and that in the fan of a growing crack in a doubly grooved tensile specimen is the relatively smaller rotation rate here in the shear band, not the sign as erroneously reported by McClintock [8]. Equations 3, 4 and 5 define the fracturing angle $2\omega_f$ uniquely for a given normal stress σ and the slip line angle λ. For this macroscopic flow field, then, we take ω_f to be a material parameter.

(c) *The apparent crack ductility, A_{CD}.*

The ratio of projected area exposed by sliding off to that exposed in the entire cycle, for example from O to O‴, is called the apparent crack ductility, A_{CD}:

$$A_{CD} = R\,\dot{\phi}\cos\lambda/(R\,\dot{\phi}\cos\lambda + \dot{c}) = \tan\omega_f \cot\lambda. \qquad (6)$$

For $\lambda = \pi/4$ this is the 'crack propagation ductility' defined by McClintock [8]. The definition given here has the advantage that the apparent ductility is observable metallographically. For instance with n parabolic dimple markings per unit area, each having tip radius r, the apparent crack ductility

may be found by assuming that the area πr^2 of each parabola opens up before arrival of the crack front, and the balance of the surface is formed by sliding off. Then

$$A_{CD} = 1 - n\pi r^2 \tag{7}$$

(d) *Geometrical changes on bending*

Because the slip surfaces meet a free surface only at the tip of the groove, the shape of the shoulders is constant until crack closure. The total change in the load-carrying dimension of the ligament, $2L^P$, is the sum of the algebraic changes measured from a coordinate system fixed in the ligament:

$$d(2L^P)/d\phi = dl_f/d\phi + dl_c^P/d\phi. \tag{8}$$

The increase of the load-carrying part of the ligament due to closing is found from the geometry of Fig. 1 and from equation 1:

$$\begin{aligned} dl_c^P/d\phi &= R\{\cos\lambda + \sin\lambda \cot[\omega(s_{xc}^P) - \phi]\} \\ &= L^P\{\cot\lambda + \cot[\omega(s_{xc}^P) - \phi]\}. \end{aligned} \tag{9}$$

Likewise the change due to fracturing is

$$dl_f/d\phi = -L^P(\cot\lambda + \cot\omega_f). \tag{10}$$

Adding equations 9 and 10 gives the change in the half-thickness of the load-carrying part of the ligament:

$$d(2L^P)/d\phi = L^P\{\cot[\omega(s_{xc}^P) - \cot\omega_f\}. \tag{11}$$

The change in the load carrying coordinate relative to the shoulders on the closing stroke, s_{xc}^P, is needed to determine the current flank angle in equation 11. It is found by determining the motion of the coordinate relative to the ligament, taking the component of that relative to the shoulder coordinates, and adding the relative motion of the ligament, coordinates to the shoulder coordinates, using the radius of the slip line from equation 1:

$$ds_{xc}^P/d\phi = L^P\{\cot[\omega(s_{xc}^P) - \phi]\cos\phi - \sin\phi\}. \tag{12}$$

Equations 11 and 12 must be integrated simultaneously. On the fracturing side the change in shoulder coordinate can now be found from an equation similar to equation 12:

$$ds_{xf}/d\phi = L^P(\cot\omega_f \cos\phi + \sin\phi). \tag{13}$$

The un-fractured thickness of the ligament, $2L^F$, is found by integrating the decrease in ligament thickness, which arises entirely from the fracturing side, equation 10, since on the closing side the crack tip remains fixed in the ligament:

$$2\bar{L}_n^F = 2\bar{L}_{n-1}^F - (\cot\lambda + \cot\omega_f)\int_{\phi_{n-1}}^{\phi_n} L^P d\phi. \tag{14}$$

For further cycling the flank angle is needed as a function of shoulder coordinate. For those coordinates at which there was fracture during this half cycle, set

$$\omega(s_x) = \omega_f - \phi \ (s_x = s_{xf}) \text{ for } s_{xf}(\phi_{n-1}) < s_x < s_{xf}(\phi_n). \tag{15}$$

From Fig. 1, the closed part of the crack extends backward from the closure point by the amount of the cracked ligament projected on the shoulder coordinates, found from equations 11 and 14. In this region, set the flank angle equal to the final bend angle of that half cycle:

$$\omega(s_x) = \phi_n \text{ for } s_{xc}(\phi_n) - (2L_n^P - 2L_n^F)\cos\phi_n < s_x < s_{xc}(\phi_n). \tag{16}$$

(a) *Repeated bending*

On reversal of bending direction, initially give the new load-carrying ligament the numerical value of the previous unfractured ligament dimension, since the crack will immediately open up:

$$L_{n+1}^P = L_n^F. \tag{17}$$

For further evaluation of equations 11 and 16, interchange the numerical values of s_{xc} and s_{xf}, and change the sign of the bend angle but leave its increments positive. Change the sign of equations 12 and 13 for the shoulder increments.

When the bend angle can be assumed small compared with both unity and the fracture angle ω_f (and hence through equation 15 small compared with any flank angle being closed the first time), equation 11 indicates that the ligament thickness remains constant to $O(\Delta\phi^2)$ over a half cycle. Equations 12-14 can now be integrated with equation 17 to give

$$(\Delta s_{xc}^P)_n = L_n^P[(\cot\omega_f)\Delta\phi_n - (\phi_n\Delta\phi_n - \Delta\phi_n^2/2) + O(\Delta\phi^3], \tag{18}$$

valid if no previously closed part is being closed a second time, and

$$(\Delta s_{xf})_n = L_n^P[(\cot\omega_f)\Delta\phi_n + \phi_n\Delta\phi_n - \Delta\phi_n^2/2 + O(\Delta\phi^3)], \tag{19}$$

$$2L_{n+1}^P/2L_n^P = 2L_n^F/2L_n^P = 1 - (\cot\lambda + \cot\omega_f)\Delta\phi_n/2 + O(\Delta\phi^2). \tag{20}$$

The mean slope of the surface being cracked can be found from equations 17, 19, and 20 by considering the s_x projections of the closed and as-fractured portions of the striations, found with the aid of Fig. 3 in terms of $A \equiv \cot\lambda + \cot\omega_f$:

$$C_x = (s^P_{xc} - s^F_{xc})_n = 2L^P_n - L^P_{n+1} = 2L^P_{n-1}(A\,\Delta\phi_n/2 - A^2\,\Delta\phi_n\,\Delta\phi_{n-1}/4 + O(\Delta\phi^3)),$$

$$F_x = (\Delta s_{xf})_{n-1} - (\Delta s^P_{xc})_n = L^P_{n-1}[\cot\omega_f)(\Delta\phi_{n-1} - \Delta\phi_n) - \Delta\phi_{n-1}(\phi_n - \Delta\phi_n) + \phi_n\Delta\phi_n - (\Delta\phi_{n-1})^2/2 - (\Delta\phi_n)^2/2 + A\cot\omega_f\,\Delta\phi_n\,\Delta\phi_{n-1}/2 + O(\Delta\phi^3)]. \quad (21)$$

The mean flank angle for the half cycle on the surface just closed, $\bar{\omega}_{nc}$, can be obtained by geometry:

$$\tan\bar{\omega}_{nc} = (F_x\tan\omega_f + C_x\tan\phi_n)/(C_x + F_x). \quad (22)$$

For cycling between fixed limits, $\Delta\phi_n = \Delta\phi_{n-1}$, equation 22 is

$$\tan\bar{\omega}_{nc} = \phi_n + \Delta\phi_n/2. \quad (23a)$$

Note that the fracture angle does not appear. It does if $\Delta\phi_n < \Delta\phi_{n-1}$, so that equation 22 becomes

$$\tan\bar{\omega}_{nc} = 1/[\cot\omega_f + (\cot\omega_f + \cot\lambda)/(\Delta\phi_{n-1}/\Delta\phi_n - 1)]. \quad (23b)$$

From equation 21, the ratio of as-fractured to total projected area for $\Delta\phi_n = \Delta\phi_{n-1}$ is

$$F_x/(C_x + F_x) = (\cot\omega_f)\,\Delta\phi_n/2, \quad (24a)$$

while for $\Delta\phi_n < \Delta\phi_{n-1}$,

$$F_x/(C_x + F_x) = 1/[1 + (1 + \tan\omega_f\cot\lambda)/(\Delta\phi_{n-1}/\Delta\phi_n - 1)]. \quad (24b)$$

Equations 23 and 24, along with equation 20 for the crack growth per cycle and equation 6 for the apparent crack ductility, provide the correlation between directly observable parameters.

Experiments

The first experiments were run on 1100-F aluminum (Rockwell hardness R_H70, Bhn≈33) to provide high ductility. To keep the features large compared with the microstructure, an initial ligament thickness of 1 in was

machined into a 3 in dia. bar with grooves having 30° flank angles. Two different limits of bend angles were used, giving fracture in about 15 cycles, with a fracture appearance as shown in Fig. 4. The experimental and theoretical results are compared in Tables 1 and 2. While the agreement is good for the angles of the re-closed and overall surfaces, the various estimates of the fracture half-angle, ω_f, leave much to be desired. It is not clear how much of these differences are due to the broadening of the slip line due to strain-hardening, and how much to blunting, some of which may be observed in the left-hand surface of Fig. 4 (see also (9)).

In order to reduce the blunting effects shown by the very ductile 1100 aluminum, other specimens were made of 1020 steel. The cold-finished steel, with a Rockwell hardness of R_B 86, (Bhn≈ 170), fractured along one of the arcs of the slip line field. An annealed specimen, R_B 64 (Bhn≈ 114), fractured along the central plane. The overall fracture was no more than a few degrees, as expected from the small bend half-angles from −3° to +3°. The fracture half-angle ω_f, deduced from the ligament ratio per half cycle of 0·557, was 7°. That deduced from the ratio of as-fractured to total projected area, 0·145 to 0·222, is 21° to 14°. The surface was too rough and porous for visual observation. Observations in an optical stereo microscope indicated an apparent crack ductility of virtually 100%, corresponding to $\omega_f \approx 0°$. All those values are less than for the more ductile 1100 aluminum, as expected, but still are not self-consistent.

Conclusion

While the angles of the overall and as-closed surfaces are well predicted, further study of the fracture angle is required, including a step decrease in amplitude during the test. Fatigue crack growth can be predicted in very low cycle fatigue under deformation-controlled bending, especially if the analysis is extended to include closure of faces cracked several cycles previously.

For studying changes in normal stress on the slip plane, the singly-grooved bending specimen is likely to be even more susceptible to blunting, suggesting that tension-compression of asymmetrically or unequally grooved specimens will be more promising.

Acknowledgement

The support of the National Science Foundation through Grant GK1875-X and a NATO Fellowship are gratefully appreciated.

References

1. RICE, J. R. & ROSENGREN, G. F. 'Plane strain deformation near a crack tip in a power law hardening material', *J. Mech. Phys. Solids*, vol. 16, p. 1, 1968.
2. HUTCHINSON, J. W. 'Singular behavior at the end of a tensile crack in a hardening material', *J. Mech. Phys. Solids*, vol. 16, p. 13, 1968.

3. McCLINTOCK, F. A. 'The growth of fatigue cracks under plastic torsion', Proc. Int. Conf. Fatigue of Metals, Inst. Mech. Eng., p. 538, 1956.
4. McCLINTOCK, F. A. 'Effects of root radius, stress, crack growth, and rate on fracture instability', Proc. Roy. Soc. A 285, p. 58, 1965.
5. GREEN, A. P. 'The plastic yielding of notched bars due to bending', *Quart. J. Mech. Appl. Math.*, vol. 6, p. 223, 1953.
6. McCLINTOCK, F. A. & ARGON, A. S., eds.'The mechanical behavior of materials', Addison-Wesley, Reading, Mass., p. 378, 1966.
7. ROGERS, H. C. 'Tensile fracture of ductile metals', *Trans. Met. Soc. A.I.M.E.*, vol. 218, p. 498, 1960.
8. McCLINTOCK, F. A. 'Local criteria for ductile fracture', *Int. Symp. Fracture Mech.*, Kiruna, Sweden, 1967, *Int. J. Fracture Mech.*, vol. 4, p. 101, 1968.
9. JOYCE, J. A. 'Tensile plastic deformation at notch roots', S.M. Thesis, Dept. of Mech. Eng., M.I.T., 1968.
10. HILL, R. 'The mathematical theory of plasticity', Oxford University Press, p. 136, 1950.

Appendix: symmetric bending with a fan

The slip line field for a doubly grooved plane strain specimen in bending has a fan at either side of the tip of the crack, as shown in Fig. 5, whenever the half-angle of the groove is $30{\cdot}0° < \omega < 73{\cdot}6°$ [5]. The half-angle λ of the central arcs is found by applying the equilibrium equation for the change in mean normal stress along LMPN; from $\sigma/2k = 1/2$ at L to O at N:

$$\lambda = 3\pi/8 + 1/4 - \omega/2. \tag{A1}$$

The radius of the central arcs is found by projecting that and the fan radius s onto the ligament:

$$R/L = [1 - (s/a)\cos\lambda]/\sin\lambda. \tag{A2}$$

The fan radius s, is that which minimizes the bending moment:

$$s/L = \frac{(2\lambda\cot\lambda - 1)/\sin\lambda}{2\lambda\cot^2\lambda - 2\cot\lambda + 2\lambda}. \tag{A3}$$

In the fan the Geiringer equations [10] show that the displacements $\dot{u}_\alpha$ are constant along the straight radial lines and thus

$$\dot{u}_\alpha = \dot{\phi}\, R_\theta \cos(\theta - \lambda - \delta), \tag{A4}$$

where the geometry of Fig. 5 gives the radius

$$R_\theta = [R + s\sin(\theta - \lambda)]/\cos\delta, \tag{A5}$$

in terms of an angle

$$\delta = \tan^{-1}[(1 - \cos\theta)/(R_\theta/s + \sin\theta)]. \tag{A6}$$

The u_β component of displacement is found by integrating a Geiringer equation with equations A4-A6.

The resulting strain fields are small except for the discontinuity along the line OP. There the direction between the displacement rate for the material near O in the triangular region at the flank of the crack and the line OP is given by:

$$\epsilon = \tan^{-1}(-\dot{u}_\beta/\dot{u}_\alpha) - (3\pi/4 - \omega). \tag{A7}$$

Values of ϵ vary from $\epsilon = 1{\cdot}1°$ to $2{\cdot}0°$ over the range of ω. Because these angles are so small for all but the most blunt cracks, it is reasonable to approximate the slip line field by the single pair of circular arcs as in the text.

Table 1
Final striation angles of 1100 aluminum

	Final overall angles, degrees			
	Symmetric bending		*Asymmetric bending*	
	n even	*n odd*	*n even*	*n odd*
Theoretical	7 1/2°	7 1/2°	2 1/2°	7 1/2°
Experimental	10 to 11	7 to 8	2 to 4	8 to 9

	Final angle of re-enclosed surfaces, degrees			
	Symmetric bending		*Asymmetric bending*	
	n even	*n odd*	*n even*	*n odd*
Theoretical	5°	5°	0°	5°
n=3	–	5 to 6	–	3 to 6
4	3 to 4	–	−4 to −2	–
5	–	5 to 6	–	5 to 7
6	6 to 9	–	1 to 4	–
7	–	5 to 6	–	2 to 4

Table 2
Estimates of fracture half-angle, ω_f, for 1100–F aluminum

Range of bending half-angle, ϕ_n	0° to 5°	−5° to 5°
ω_f estimated from stereograms from scanning microscope		35°– 40°
ω_f observable from depth of field in optical stereomicroscope (9 readings)		35°– 42°
Ligament shrinkage		
L_n/L_{n-1} (5 half cycles)	·81	69
ω_f from equation 20	14	18
Apparent crack ductility		
A_{CD} from scanning microscope		9 – 1
ω_f from equation 6		64°– 67°
As-fractured appearance		
$F_x/(C_x + F_x)$ (8 and 5 readings, resp.)	·11 – ·16	·14°– ·25°
ω_f from equation 24a	22°– 16°	33°– 20°

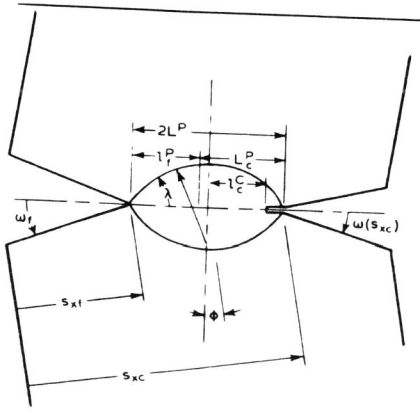

Fig. 1. Simultaneous opening and closing in bending.

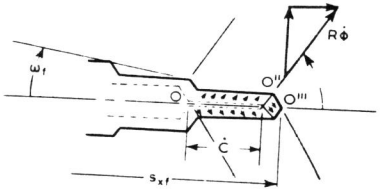

Fig. 2. Crack growth-alternating slip with cleavage.

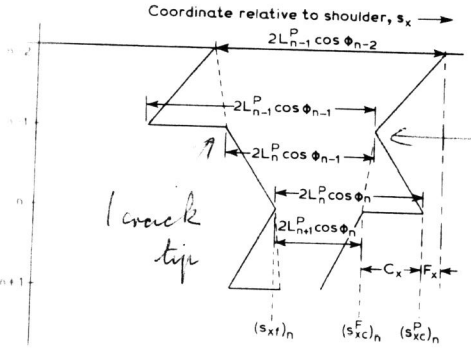

Fig. 3. Shift of crack tip during cycling.

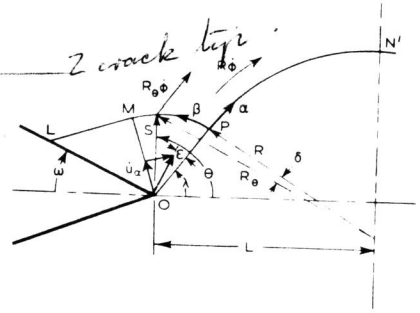

Fig. 5. Slip line field for bending with a fan.

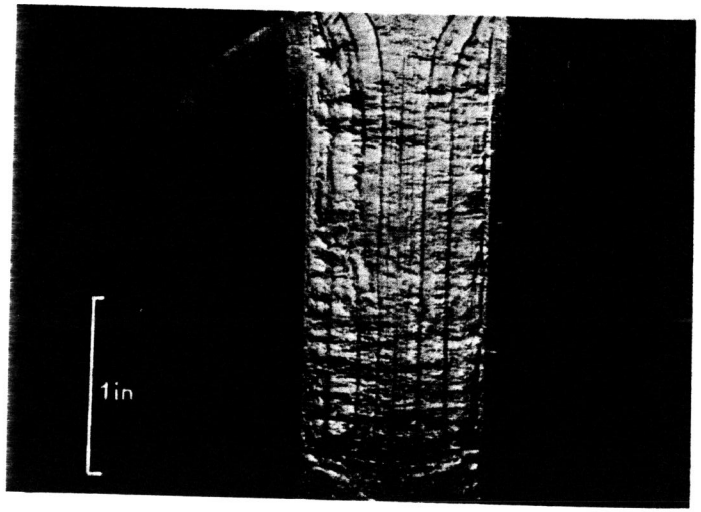

Fig. 4. Fracture surface in 1100°F aluminum. $\phi = -5°$ to 5°.

Take assume this amount fractures ahead of crack tip

This fractures by sliding off.